10.5 W Time-Averaged Power Mid-IR Supercontinuum Generation Extending Beyond 4 μm With Direct Pulse Pattern Modulation

Chenan Xia, Zhao Xu, Mohammed N. Islam, *Fellow, IEEE*, Fred L. Terry, Jr., *Senior Member, IEEE*, Mike J. Freeman, Andy Zakel, and Jeremiah Mauricio

***Abstract*—A novel, all-fiber-integrated supercontinuum (SC) laser is demonstrated and provides up to 10.5 W time-averaged power with a continuous spectrum from ~0.8 to 4 μm. The SC is generated in a combination of standard single-mode fibers and ZrF_4–BaF_2–LaF_3–AlF_3–NaF (ZBLAN) fluoride fibers pumped by a laser-diode-based cladding-pumped fiber amplifier system. The output SC pulse pattern can be modulated by directly modulating the seed laser diode. Near-diffraction-limited beam qualities are maintained over the entire SC spectrum. The SC average power is also linearly scalable by varying the input pump power and pulse repetition rate. We further investigate the theoretical limitations on the achievable average power handling and spectral width for the SC generation in ZBLAN fibers. Based on the thermal modeling, the standard ZBLAN fiber can handle a time-averaged power up to ~15 W, which can be further scaled up to ~40 W with a proper thermal coating applied onto the ZBLAN fiber. The SC long-wavelength edge is limited by the nonlinear wavelength generation processes, fiber bend-induced loss, and glass material loss. By using a ZBLAN fiber with a 0.3 numerical aperture, the SC spectrum could extend out to ~4.5 μm, which is then limited by the material loss.**

***Index Terms*—Fiber laser, mid-IR, modulation, supercontinuum (SC).**

I. Introduction

SUPERCONTINUUM (SC) generation process, in which the spectrum of a narrow bandwidth laser undergoes a substantial spectral broadening through the interplay of different nonlinear optical interactions, has been widely reported and studied since it was observed in 1969 [1]. Recently, broadband SC generation in optical fibers is of particular interest because of the optical fibers' unique advantages in their long optical interaction length, high nonlinearity, and potential applications in the optical telecommunication [2], [3]. For example, a soft-glass (Schott SF6) photonics crystal fiber (PCF) has been used to generate and extend the SC spectrum down to ~350 nm in the deep blue regime [4]. Also, various techniques have been used to demonstrate SC generation with the long-wavelength edge reaching as far as ~3 μm [4], [5], which is then limited by the soaring material absorption of the silica glass [6]. Recently, the time-averaged power of the SC in the PCF fiber has also been increased to 50 W [7].

A high-power all-fiber-integrated mid-IR SC light source has applications in a variety of areas. Conventional mid-IR laser sources, including optical parametric amplifiers (OPAs) [8], quantum cascaded lasers [9], synchrotron lasers [10], and free electron lasers [11], are used in IR countermeasures [9], free-space communications [9], and optical tissue ablation [12]. In comparison, SC lasers have no moving parts, output in single spatial mode, and operate at room temperature. In addition, the fiber-based SC source can generate a broad spectrum covering the entire near- and mid-IR regime simultaneously, which can improve both the sensitivity and selectivity of remote chemical sensing [13] and real-time optical metrology [14]. Finally, direct signal modulation functionality is also desirable for SC laser sources to eliminate the need for external signal modulation or chopping equipment, which is difficult to implement in the mode-locked lasers-based systems [15], [16].

To generate SC spectrum in the mid-IR, optical fibers with low loss in the mid-IR windows, such as chalcogenide, fluoride, and tellurite, are required. For example, spectrum shifting from 1.55 to ~1.9 μm is reported in the chalcogenide fibers, where further wavelength redshifting is limited due to the low optical damage threshold of ~1 GW/cm^2 and high normal dispersion [17]. SC generation ranging from 2 to 3 μm has also been demonstrated in sulfide and selenide fibers by a 2.5-μm OPA pump laser [18]. On the other hand, mode-locked femtosecond lasers have been used to generate SC spectrum beyond 3 μm in both fluoride [15] and tellurite fibers [16] with modest average power (<0.1 W). We have also developed a ZrF_4–BaF_2–LaF_3–AlF_3–NaF (ZBLAN) fluoride-fiber-based laser source to provide an SC spectrum ranging from ~0.8 to ~4.5 μm [19], and we have scaled up the time-averaged output power to 1.3 W by using cladding-pumped fiber amplifiers in a tabletop system [20].

In this paper, we describe an all-fiber-integrated SC laser that can provide a time-averaged output power scalable up to 10.5 W

Manuscript received October 1, 2008; revised October 31, 2008. Current version published April 8, 2009. This work was supported in part by the Army Research Office under Project W911NF-04-C-0078, by the Defense Advanced Research Projects Agency (DARPA) under Project W31P4Q-05-C-0159, and by Omni Sciences, Inc. Laboratory equipment for this work was funded by Vyalex, Inc., through a contract from the Naval Air Command (NAVAIR) PMA-272.

C. Xia, Z. Xu, and F. L. Terry, Jr., are with the Department of Electrical Engineering and Computer Science, University of Michigan, Ann Arbor, MI 48109 USA (e-mail: caxia@umich.edu).

M. N. Islam is with the Department of Electrical Engineering and Computer Science, University of Michigan, Ann Arbor, MI 48109 USA, and also with Omni Sciences, Inc., Ann Arbor, MI 48105 USA (e-mail: mni@eecs.umich.edu).

M. J. Freeman, A. Zakel, and J. Mauricio are with Omni Sciences, Inc., Ann Arbor, MI 48105, USA.

Color versions of one or more of the figures in this paper are available online at http://ieeexplore.ieee.org.

Digital Object Identifier 10.1109/JSTQE.2008.2010233

1077-260X/$25.00 © 2009 IEEE

Authorized licensed use limited to: IEEE Xplore. Downloaded on April 24, 2009 at 15:54 from IEEE Xplore. Restrictions apply.

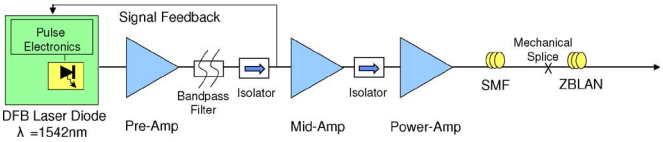

Fig. 1. High-power all-fiber-integrated SC laser setup.

in the mid-IR with direct pulse pattern modulation capability. The SC extends beyond 4 μm in ZBLAN fibers with an average output power of 10.5 W—the highest SC power reported to date in the mid-IR fibers. In addition, the average output power of the SC laser is linearly scalable with respect to the total pump power by varying the pulse duty cycle while maintaining the similar spectral shape. For the first time to our knowledge, we also demonstrate pulse pattern modulation of the SC by directly modulating the seed laser diode and controlling the amplifier gain with signal feedback technique. Our SC laser can output a modulated pulse pattern with the duty cycle adjustable from nominally 0% to 100%. Therefore, our SC laser has no moving parts, covers the near- and mid-IR spectrum, and eliminates the need for mode-locked lasers.

The pump system of the SC laser comprises a 1542-nm laser diode generating 1 ns pulses, followed by a single-mode erbium-doped fiber amplifier (EDFA) and multistage cladding-pumped erbium/ytterbium codoped fiber amplifiers (EYFAs). Optical spectrum of the amplified nanosecond pulses is then broadened in a combination of 2 m length of standard single-mode fiber (SMF) followed by 7 m length of the ZBLAN fiber. Numerical simulations are also carried out to investigate the power and spectral bandwidth limit of the SC generation in ZBLAN fluoride fibers. We show that the maximum SC average power to be handled in a given fiber is constrained by thermal effects. Up to $\sim$15 W, SC can be generated in standard ZBLAN fibers, while $\sim$40 W SC is achievable by applying a thermal coating onto the fiber to dissipate the heat. The long-wavelength edge of the SC is limited by the combination of fiber bend-induced loss, fluoride material loss, and ZBLAN fiber nonlinearities. By designing a ZBLAN fiber with a core size of 7 μm and a numerical aperture (NA) of 0.3, the SC long-wavelength edge can be extended to $\sim$4.5 μm, which is then limited by the material absorption loss.

This paper is organized as follows. We describe the SC laser setup in Section II and experimental results of the SC generation in Section III. In Section IV, we demonstrate the pulse pattern modulation of our SC laser. In Section V, we study the power limitation of the SC generation in ZBLAN fibers. The theoretical results are verified by our experimental data. We also project the potential achievable output power of the SC generation in ZBLAN fiber. In Section VI, we study the long-wavelength edge of the SC generation in ZBLAN fibers, and propose a ZBLAN fiber design to extend the SC long-wavelength edge to $\sim$4.5 μm. Finally, we discuss and summarize the experimental and simulation results in Section VII.

II. Experimental Setup

The experimental setup is illustrated in Fig. 1. A 10-mW distributed feedback (DFB) laser diode emitting at 1542 nm is driven by electronic circuits to provide 400 ps to 2 ns pulses at variable repetition rate. The electronic circuits can also drive the laser diode to output a preprogrammed pulse pattern instead of fixed repetitive pulses. Details of the pulse pattern modulation will be described in Section IV. The optical pulses are amplified by three stages of fiber amplifiers—an EDFA preamplifier followed by EYFA mid-stage and power amplifiers. The preamplifier uses a 1 m length of 4/125 μm (core/cladding diameter) single-mode erbium-doped gain fiber, and the mid-stage amplifier employs a 1.5 m length of 7/125 (core/cladding diameter) cladding-pumped gain fiber. In a multistage amplifier, the noise performance, i.e., amplified spontaneous emission (ASE), is determined by the upstream stages before the power amplifier. To lower the ASE, we separate the amplifier into one preamplifier and one mid-stage amplifier. Therefore, the ASE after the first stage can be filtered by a 100-GHz bandpass filter, and the signal gain in each amplifier stage can be reduced. Optical isolators are also placed between the stages to protect the system from back-reflection damage as well as to reduce the noise figure and improve the efficiency of the combined amplifier system. Under typical operating conditions, we obtain $\sim$20 dB gain in both the pre- and mid-amplifier for the optical signal while the ASE-to-signal ratio is measured to be less than 1%. The nonlinear broadening of the optical pulses before the power amplifier is also negligible. In addition, a 1% optical tap is used to sample the output power of the preamplifier and enable the signal feedback control, which is described in detail in Section IV.

The power from the mid-amplifier is boosted in an all-fiber-spliced, cladding-pumped EYFA before coupling into the SC fiber. A cladding-pumped fiber amplifier is required to increase the gain volume and enable the coupling of multiple pump diodes. In addition, to minimize the nonlinear effects in the amplifier, a short length of gain fiber with a large core diameter and a high doping concentration is used. For the 10 W SC generation experiment, we have designed a gain fiber with a core diameter of 15 μm and an effective NA of 0.15, whose mode field is close to that of the SMF fiber. The EYFA has an $\sim$5 m length of gain fiber with a 15/200 μm core/cladding diameter and a 2 dB/m absorption at 915 nm. Ten 8-W 976-nm and two 8-W 940-nm uncooled multimode pump diodes are coupled into the gain fiber through an 18×1 pump combiner. Single spatial mode operation is maintained in the EYFA by carefully splicing the gain fiber to the signal-input SMF fiber and the pump combiner. By pumping the system with $\sim$75 W average power in the counterpropagation configuration, the EYFA can provide $\sim$20.2 W average power output after a 2 m length of SMF fiber is spliced to the output of the gain fiber. This corresponds to $\sim$6.1 kW peak power ($\sim$15 dB signal gain) for 1 ns pulses at a 3.33-MHz repetition rate and $\sim$27% pump-to-signal conversion efficiency. The output spectrum after the SMF fiber is broadened and redshifted to $\sim$2.2 μm primarily due to the break up of the nanosecond pulses through modulation instability (MI) followed by soliton self-frequency shifting [5]. The pump-to-signal conversion efficiency is slightly lower than the usual 30%–35% figure because of the high-peak-power-induced nonlinear wavelength generation in both the fiber amplifier and SMF.

Authorized licensed use limited to: IEEE Xplore. Downloaded on April 24, 2009 at 15:54 from IEEE Xplore. Restrictions apply.

For the SC modulation experiment, we use a 12/130 μm core/cladding diameter erbium/ytterbium codoped fiber with a 0.20 NA as the gain fiber in the final stage power amplifier. We reduce the length of the gain fiber to $\sim$4 m because the 940 nm pump cladding absorption is increased to $\sim$3.3 dB/m. Four 6 W, 940 nm pump diodes are coupled into the gain fiber through a 6×1 pump combiner. We generate $\sim$6 W ($\sim$10 kW) average (peak) output power after $\sim$2-m-length SMF fiber when the seed laser is operated at 1.54 MHz repetition rate with $\sim$400 ps pulse duration.

We generate the SC in a two-stage process. In the first-stage SMF fiber, we utilize MI to break up the nanosecond pulses into femtosecond pulse trains to enhance the nonlinear optical effects and redshift the optical spectrum to beyond 2 μm [5]. The SC spectrum is then broadened in the following ZBLAN fiber through the interplay of self-phase modulation (SPM), Raman scattering, and parametric four-wave mixing (FWM) [5], [20].

SC is generated by butt-coupling the light from the 2 m length of SMF fiber after the EYFA into a piece of ZBLAN fluoride fiber. Two ZBLAN fluoride fibers are used in the experiments. In the 10.5-W high-power SC experiment, the ZBLAN fiber we designate as FL#1 is 7 m long and has a core diameter of 8.9 μm, a cladding diameter of 125 μm, and an NA of 0.21. The ZBLAN fiber we call as FL#2 is used in the SC modulation experiment and has a length of $\sim$15 m with a core diameter of 10.6 μm, a cladding diameter of 125 μm, and an NA of 0.2. All ends of SMF and ZBLAN fibers are angle cleaved to avoid light back reflected into the pump system. To improve the coupling stability and heat dissipation capacity, each end of the butt-coupling fibers, i.e., SMF and ZBLAN fibers, is mechanically clamped onto an aluminum v-groove, and the fiber claddings are covered with a high refractive index optical glue to remove the residual cladding modes. The SC spectrum between 500 and 1750 nm is measured by an optical spectral analyzer, while the spectral information ranging from 1750 to 4500 nm is acquired using a Czerny–Turner monochromator and a liquid-nitrogen-cooled InSb detector.

III. 10.5 W SC Generation in ZBLAN Fibers

Mid-IR SC with a time-averaged power of 10.5 W and a continuous spectrum of $\sim$0.8 to more than 4 μm is generated by pumping an $\sim$2 m length of SMF fiber followed by $\sim$7 m length of the ZBLAN fluoride fiber (FL#1) with the amplified nanosecond pulses, as illustrated in Fig. 2. The generated SC is smooth and relatively flat across the majority of the spectrum with a spectral power density $>$0 dBm/nm (1 mW/nm). The measured SC spectrum is corrected for the spectral responsivity of the InSb detector. The spectral power density is then calculated by using the total SC output power measured by the thermal power meter. The pump to SC conversion efficiency in the ZBLAN fiber is $>$50%, i.e., 10.5 W of SC output/20.2 W output of the SMF fiber. The SC average power beyond 1600, 2500, and 3000 nm is measured to be $\sim$7.3, $\sim$3.0, and $\sim$1.1 W, respectively, by using long-pass filters with the corresponding cutoff wavelengths. The residual power in the 1550 nm pump wavelength is less than 0.1 W. The average power of the SC is

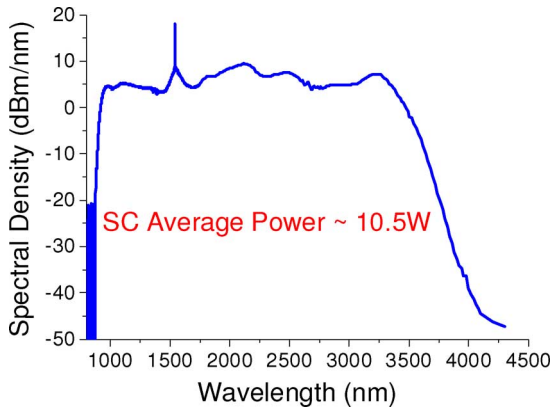

Fig. 2. SC spectrum for 2 m SMF followed by $\sim$7 m ZBLAN fiber (FL#1).

currently limited by the available pump power from the fiber amplifiers. The long-wavelength edge of the SC is primarily limited by the length of the ZBLAN fiber in conjunction with other optical effects, including the fiber bend-induced loss and ZBLAN material absorption [19], [20]. Detailed discussion and analysis on the limitation of SC spectral bandwidth is carried out in Section VI.

For a given fiber, there are three adjustable parameters in our SC light source, which are pulsewidth, repetition rate, and pump power. To obtain the maximum SC power in the mid-IR and generate the broadest spectrum, all three parameters should be optimized. The laser pulsewidth is set based on the following two criteria. First, the pulsewidth shall be short enough to mitigate any transient thermal effects in the optical fiber. On the other hand, a nanosecond pulse scale is also preferable for the intrapulse nonlinear interaction and spectrum broadening. Therefore, we drive our DFB laser diode with the pulsewidth in the range of 0.4–2 ns. Furthermore, the pulse repetition rate couples with the pulsewidth to determine the duty cycle of the laser system. Since the DFB laser diode pulses remove the energy provided by the EYFA pump lasers of the power amplifier of the SC system in the time between DFB pulses, the peak output power varies inversely with the pulse duty cycle with a fixed pump power supply. In other words, the peak output power increases with the reduction of the pulse repetition rate, i.e., pulse duty cycle, and vice versa.

Fig. 3 shows the average power of SC spectral components beyond 3000 nm for varying pulse repetition rate with four 976 nm pump diodes. As can be seen, the total SC spectral power beyond 3000 nm increases from $\sim$0.19 to $\sim$0.48 W by reducing the pulse repetition rate from 1.33 to 0.67 MHz. We attribute the increase of spectral power to the boost of the peak power coupled into the SMF and ZBLAN fibers to enhance the nonlinear SC generation process [5], [20]. However, the SC power beyond 3000 nm drops down to $\sim$0.26 W when we further decrease the repetition rate to 0.25 MHz. The drop of the SC spectral power can be caused by the increased power loss in the SC long-wavelength edge and reduced amplifier conversion efficiency in the low duty cycle operational condition. Since the SC long-wavelength edge is limited by the loss of the fiber, including both bend-induced loss and fluoride material loss, the

Authorized licensed use limited to: IEEE Xplore. Downloaded on April 24, 2009 at 15:54 from IEEE Xplore. Restrictions apply.

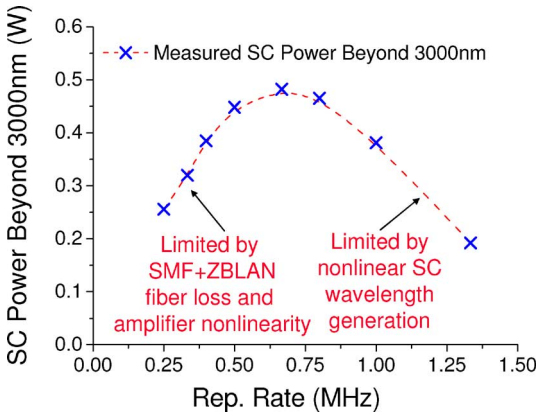

Fig. 3. Average power of SC spectral components beyond 3000 nm for varying pulse repetition rate with four 976 nm pump diodes.

additional spectrum generated in the vicinity of the SC edge by the additional peak power is heavily attenuated, which, in turn, reduces the total SC power in the mid-IR regime. In other words, despite of the fact that higher peak power could lead to more spectral broadening, such spectral components vanish during their propagation in the ZBLAN fiber and are not observed at the output end. Therefore, the SC light source should be operated at the repetition rate of 0.67 MHz in this particular case to achieve the maximum spectral output in the mid-IR.

The time-averaged power of SC is linearly scalable with respect to the input pump power without changing the spectral shape. Since the entire SC spectrum is generated in each amplified nanosecond laser pulse, which does not interact with adjacent optical pulses, the SC average power can be boosted by simply increasing the total number of the optical pulses in the given time period. To ensure the SC spectral shape is maintained, the peak power of the amplified pulses is kept the same by adjusting the pulse repetition rate and total pump power for the fiber amplifiers. As illustrated in Fig. 4(a), we scale the SC average power from 1.4 to 10.5 W by varying the pulse repetition rate proportionally from 0.42 to 3.33 MHz and increasing the pump power accordingly. The change of the SC average power is linearly proportional to the change of the pulse duty cycle, which agrees well with our hypothesis. To further confirm that the same SC spectrum shape has been generated during the change of the SC average power, the ratio of the SC spectral power beyond 2500 nm over the total SC power is measured and shown in Fig. 4(b). We observe that the ratio stays approximately constant across the entire power range, which indicates that the power generated in the mid-IR scales up proportionally to the increasing total SC power. Therefore, the output power of our SC light source can be linearly and continuously varied with respect to the input pump power while keeping the same spectral shape.

IV. Pulse Pattern Modulation of the SC Light Source

We demonstrate pulse pattern modulation of our SC source by directly modulating the seed laser diode and controlling the signal gain of the power amplifier. To modulate the SC output,

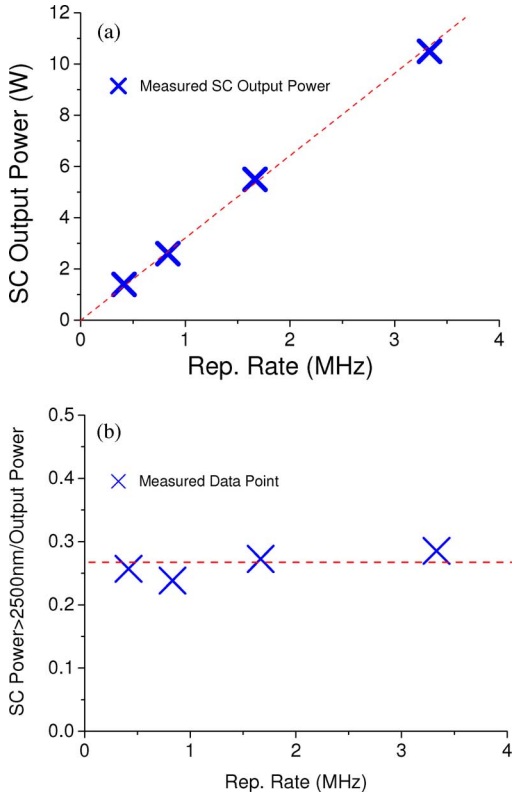

Fig. 4. (a) Average SC output power scaling by varying pulse repetition rate and pump power. (b) Ratio of the SC power of the spectral components beyond 2500 nm with respect to total SC power under different operating repetition rate.

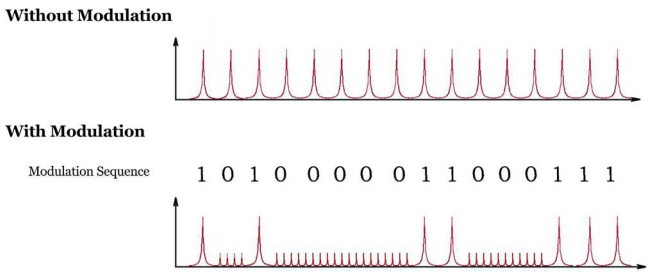

Fig. 5. Pump pulse modulation pattern (not drawn to scale). "0"/"1" represents SC OFF/ON code.

the optical pump pulses amplified by the multistage fiber amplifiers need to be temporally encoded with the desirable pulse pattern. However, constant input power level is required to saturate the amplifier during the time period of the SC-OFF coding pattern to prevent storage of excess energy in the EYFA that would otherwise damage the amplifier [21].

We modulate the SC output, i.e., turn the SC output ON/OFF, by feeding pump pulses that are temporally patterned with high/low peak power to the ZBLAN fiber. SC generation is a nonlinear optical process; thus, the broadband SC spectrum can only be generated by amplified laser diode pulses with sufficient peak power, which typically needs to be in the kilowatt range. Fig. 5 illustrates an exemplary pump pulse pattern, where a "1" code represents the one SC-ON pulse and a "0" code represents a series of SC-OFF mini-pulses. To enable the SC output, a high

Authorized licensed use limited to: IEEE Xplore. Downloaded on April 24, 2009 at 15:54 from IEEE Xplore. Restrictions apply.

peak power bearing pump pulse can be coupled into the ZBLAN fiber to generate the broadband spectrum. On the other hand, a series of mini-pulses with low peak power, which undergo minimal nonlinear broadening in the ZBLAN fiber, is used to nullify the SC output. Therefore, the SC output can be directly modulated by temporally encoding the pulse pattern onto the driving currents for gain-switching DFB seed laser diodes.

We use mini-pulses during the SC-OFF time period to saturate the power amplifier and maintain the same signal gain level for the succeeding SC-ON pump pulses. In order to keep the gain of the power amplifier the same for both SC-ON pump pulses and SC-OFF mini-pulses, the average output power of the preamplifier needs to stay unchanged. We use a feedback loop technique to continuously sample the output power of the preamplifier, and then adjust the DFB seed laser power level accordingly to maintain constant output power. The 1% optical tap for signal strength monitoring is placed after the preamplifier and the bandpass filter, but before any of the middle stage amplifier components. This allows the signal to be strong enough such that a 1% coupling still has a high SNR but avoids any significant nonlinear effects in the fiber and keeps detector saturation to a minimum. Placing the 1% tap after the 100-GHz bandpass filter assures that the signal seen by the feedback loop and the middle stage amplifier are nearly identical, since the seed laser diode puts out a much higher percentage of power into wavelengths other than 1542 nm for the mini-pulses that are barely above threshold than it does for the main pump pulses. In particular, the pulse repetition rate is set to 1.54 MHz for the SC-ON pump pulses and is switched to 50 MHz for the SC-OFF mini-pulses. Since the average power of the amplifier system remains unchanged, the peak power for the mini-pulse is reduced to $<1/30$ that of the normal pump pulse.

Fig. 6(a) shows a sample modulation pattern output of our SC source. The SC laser is operated at a base repetition rate of 1.54 MHz with pump pulse duration of 400 ps. The output power of the SC is measured to be $\sim$2.4 W unmodulated. Two pulse envelops are encoded into the SC output—one has a width of 130 μs repeating at 1.5 kHz and the other has a width of 650 μs repeating at 7.7 kHz. Therefore, the modulation pattern consists of a 200-pulse burst with a temporal duration of 130 μs, followed by an SC-OFF time of 130 μs, plus another 1000-pulse burst with a temporal duration of 650 μs, followed by an SC-OFF time of 650 μs. The resulting duty cycle is 50% of the nominal SC output with the 1.54 MHz continuous repetitive pulses. One thing to note is that the pulse trace displayed in Fig. 6(a) shows an $\sim$25% peak-to-peak variation. We attribute such amplitude variation to the limited bandwidth and memory depth of the oscilloscope used in the experiments, which leads to undersampling of each pulse in the train and uncertainties in the pulse-to-pulse variation measurement. We have also used a fast oscilloscope (500 MHz bandwidth) to measure the peak-to-peak energy variation on a single pulse in the fix repetition rate mode at 1550 and 2555 nm. The peak-to-peak power variation is estimated to be approximately 3%.

The modulated SC spectrum is plotted in Fig. 6(b) overlapping with the unmodulated spectrum. The SC spectrum shown in Fig. 6 is generated in FL#2 and has similar spectral bandwidth as that generated in FL#1. The amplitude of the SC spectrum in the modulation mode in Fig. 6 is vertically displaced to match the SC spectrum in the unmodulated mode. We observe no discernible changes in the SC spectrum in both the long- and short-wavelength sides. The spectral power remaining in the vicinity of the pump wavelength in the modulation mode is $\sim$10 dB higher than that of unmodulated mode, which could be attributed to the optical power of the SC-OFF mini-pulses. The modulated SC outputs 3.45 W in total, within which $\sim$1.2 W is estimated to be in the continuum. The measured modulated SC output correlates to the powers in the unmodulated mode with the 50% duty cycle. The residual power, i.e., 3.45–1.2 W, is composed of $\sim$1 W remaining in the pump and the rest of the power representing spectral components with small wavelength shifting in the vicinity of pump wavelength. Future work will be conducted to increase the SC-OFF pulse repetition rate beyond 100 MHz to further reduce the peak power of the mini-pulses and the corresponding nonlinear wavelength shifting.

The modulation duty cycle of our SC laser can be adjusted from nominally 0% to 100%. We estimate the saturation time of the power amplifier to be $\sim$10 μs. As previously mentioned,

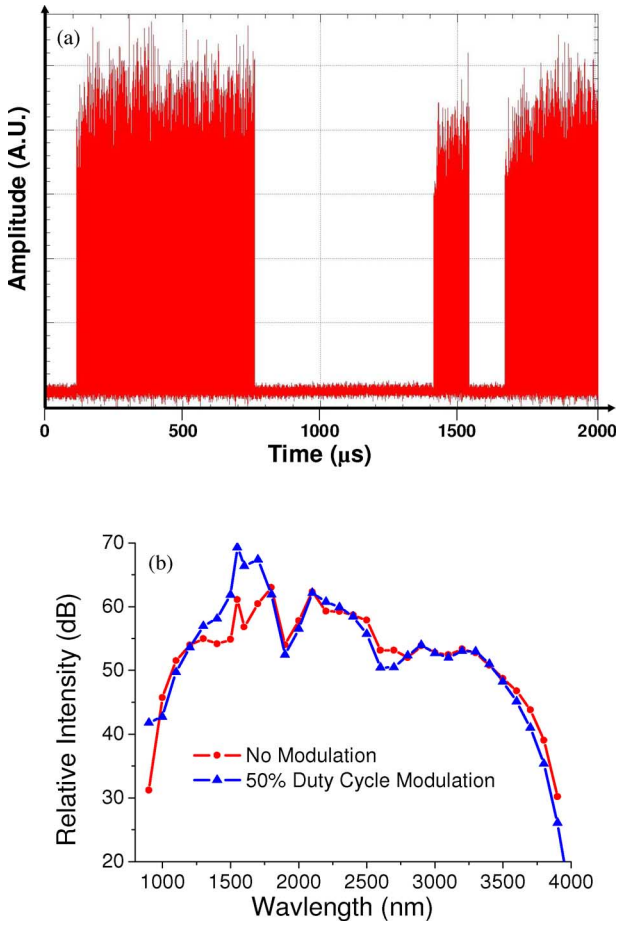

Fig. 6. SC modulation experiments. (a) Output pulse modulation pattern. The modulation pattern consists of a 200-pulse burst with a temporal duration of 130 μs, followed by an SC-OFF time of 130 μs, plus another 1000-pulse burst with a temporal duration of 650 μs, followed by an SC-OFF time of 650 μs. (b) SC spectral output in modulated and unmodulated modes.

Authorized licensed use limited to: IEEE Xplore. Downloaded on April 24, 2009 at 15:54 from IEEE Xplore. Restrictions apply.

a series of mini-pulse is injected into the power amplifier at the SC-OFF period to maintain the constant average output power of the amplifier. The switching time between regular pump pulse and mini-pulse is ~100–150 ns in our driving circuits for the seed laser diode. We also observe a slight "ramp up" region at the start of each pulse envelop in Fig. 6(a), which is due to the transient laser diode driver circuit response.

Our SC light source outputs near-diffraction-limited beam quality over the entire spectrum. To measure the beam quality of the SC spectrum, the output of the SC is first collimated by a gold-coated parabolic reflective mirror and passes through optical bandpass filters in different bands. The filtered SC light is then focused by a CaF_2 lens, and the intensity profile of the laser beam is mapped at difference axial locations around the focal spot by using a knife edge cutting across the beam. We estimate the M^2 value by fitting the beam shape to the Gaussian beam propagation profile. Fig. 7 demonstrates the M^2 measurement of the SC output beam centered at (a) 1550 nm (~10 nm bandwidth), (b) 2555 nm (~50 nm bandwidth), and (c) 3275 nm (~50 nm bandwidth), all in FL#2. The generated SC spectrum is similar to that of FL#1 with the detailed spectrum analyzed in the following section. As can been seen, all of the wavelengths exhibit near-diffraction-limited performance with M^2 approaching 1 moving toward the long-wavelength region. Such behavior could be attributed to the step-index geometry of the ZBLAN fiber, which is not strictly single spatial mode at wavelengths below the cutoff wavelength (e.g., ~2.7 μm for FL#2). The M^2 value at 3275 nm is ~0.1 higher than that at 2555 nm, which might be due to the uncertainty of the measurement or the different filter bandwidth at these two wavelengths. It should also be noted that the output of the ZBLAN fiber is end-capped with a thin ZBLAN glass slide to prevent the surface damage, which might also reduce the output beam quality of the SC at various wavelengths.

V. Power Handling Limit of the SC Generation in ZBLAN Fiber

During the experiment, the time-averaged power is limited by the available pump power from the fiber amplifier, and the SC spectral width is limited by the fiber length in combination with fiber bend-induced loss and material loss. We further model the SC generation process to explore the limits of the time-averaged power and spectral bandwidth of the SC in different optical fibers.

The maximum power handling of the optical fiber is limited by the optical material damage. For optical pulses shorter than ~10 ps, the optical damage can be attributed to the multiphoton-initiated avalanche ionization of the target glass material as reported in [22]. For optical pulses from ~50 ps to over 100 ns, joule heating of the glass material needs to be taken into consideration [23]. Furthermore, the time-averaged power handling of optical fiber is primarily limited by the heating and melting of the dielectric material, such as catastrophic destruction and fiber fuse damage, which is associated with the fiber glass melting temperature, absorption, and heat conductivity [22]–[25]. Therefore, such damage mechanism puts an upper limit to both the peak power or optical intensity of the laser pulse and the time-averaged power that the optical fiber can handle without incurring any material damage.

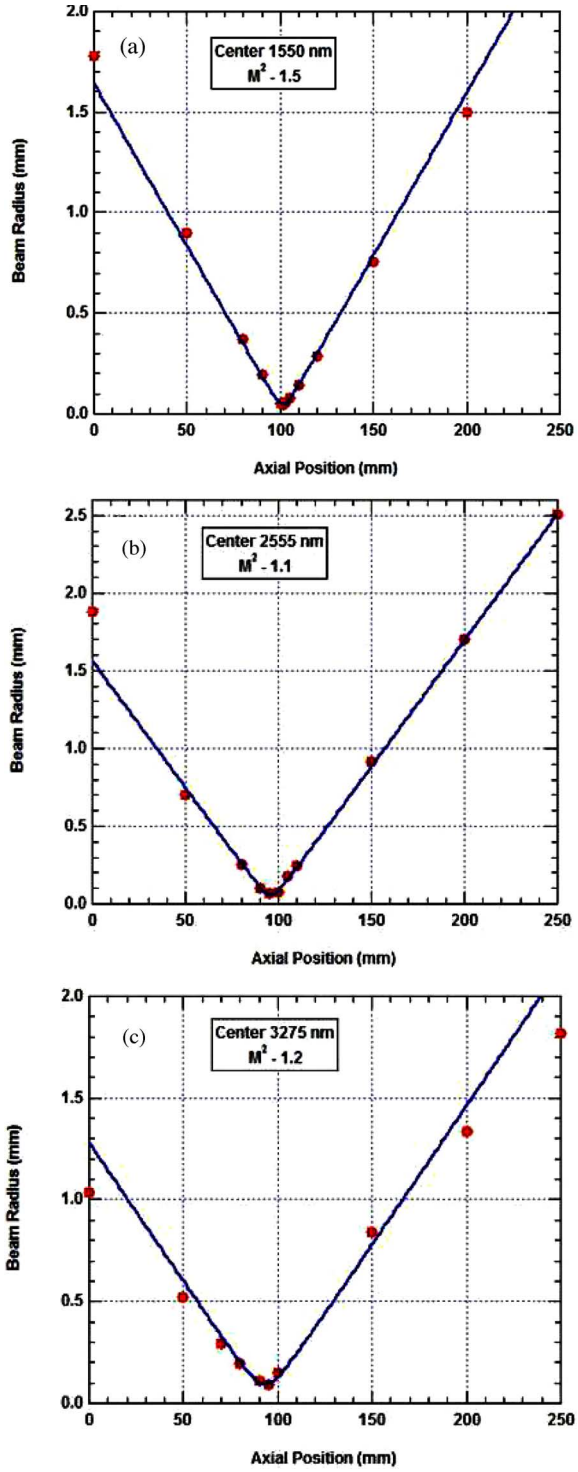

Fig. 7. Beam quality M^2 measurement. (a) 1550 nm. (b) 2555 nm. (c) 3275 nm.

We assess the laser-induced optical damage in our SC system in two subcategories: peak-power-induced and average-power-induced optical damage. For the peak-power-induced optical surface damage, the damage threshold scales inversely

Authorized licensed use limited to: IEEE Xplore. Downloaded on April 24, 2009 at 15:54 from IEEE Xplore. Restrictions apply.

proportional to the square root of the pulsewidth, i.e., $\propto\tau^{-1/2}$, for the pulses with pulsewidth larger than a few tens of picosecond. For example, the damage threshold has been measured in the fused silica to be $\sim$400 GW/cm^2 with a 10-ps pulse, and 40 GW/cm^2 with a 1-ns pulse at 1053 nm [22]. However, the $\propto\tau^{-1/2}$ dependence does not hold any more for the shorter pulses. Optical damage of the fiber occurs in a small region around the center of Gaussian distributed incident pulse due to the avalanche ionization. For the fused silica, optical damage at $\sim$11 TW/cm^2 has been observed with a pulse of 140 fs pulsewidth at 825 nm, i.e., $\sim$1.6 J/cm^2 per pulse. For the fluoride fibers, similar behaviors have been observed. The damage threshold for CaF_2 is measured to be $\sim$20 GW/cm^2 with a 1-ns pulse (corresponding to 20 J/cm^2 per pulse), and increases to $\sim$5 TW/cm^2 for a 0.4-ps pulse (corresponding to $\sim$2 J/cm^2 per pulse) [22].

Using the reported optical damage threshold for both silica and fluoride materials [22], [23], we calculate that the ZBLAN fluoride fiber with an 8.9 μm core diameter can handle $>$10 kW peak power with 1 ns pulse duration, while the single-mode silica fiber can handle $>$20 kW peak power with the same pulsewidth. In our experiments, the peak power used in the SC generation is $<$10 kW for both SMF and ZBLAN fiber, and therefore has not yet reached the limits mentioned. In particular, the peak output power is $\sim$6–8 kW in the SMF fiber and 3–5 kW in the ZBLAN fiber, both of which are lower than the projected optical breakdown limit. Although the MI-breakup pulses may possess higher peak power, the shortened pulsewidth, e.g., $\sim$100–200 fs, increases the optical damage threshold of the fibers. During the operation of our SC laser, we have not observed any peak-power-induced optical damage at the mechanical splicing point, which includes the output facet of the SMF fiber and the input facet of the ZBLAN fiber. Because the optical peak power will be kept at the same level for SC generation with different time-averaged output power, it shall not limit the development of an SC laser source with average output power higher than 10 W.

The average power handling of the optical fiber, on the other hand, is limited by the heat absorption that results in the melting of the fiber glass. The absorption coefficient of the dielectric glass increases drastically when the glass temperature rises close to the glass transition temperature. The bulk glass material will then heat up, which further increases the material absorption and leads to the melting of the fiber glass and catastrophic fuse damage. Therefore, the maximum average power handling of the fiber under a given experimental condition is limited to the situation when the temperature of the fiber core rises close to its melting point.

Since the fiber cross section is structured as Fig. 8, the fiber core temperature can be calculated by the following formula [26]:

$$T_{\text{core}} = \frac{Q}{2\pi}\left[\frac{\ln(r_{\text{cladding}}/r_{\text{core}})}{k_{\text{cladding}}} + \frac{\ln(r_{\text{thermal pad}}/r_{\text{cladding}})}{k_{\text{thermal pad}}} + \frac{1}{h_{\text{air}} r_{\text{thermal pad}}}\right] + T_{\text{air}}$$

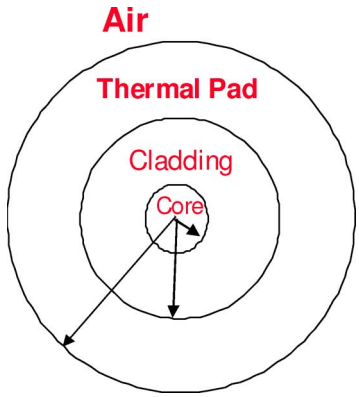

Fig. 8. Fiber cross-section structure.

where r is the radius of the respective subscript, k is the thermal conductivity, and h is the thermal convection coefficient. In addition, Q represents the power dissipation in the SC generation process in the unit fiber length and T the temperature of the respective subscript. The melting temperature of silica glass is 1448 K with a thermal conductivity of 1.38 W/(m·K) [27]. For the fluoride glass, the melting temperature is 528 K with a thermal conductivity of 0.628 W/(m·K) [27], [28]. Because the input side of the fiber possesses the highest optical power and bears the most heat dissipation, we estimate the maximum power handling of the optical fiber by calculating the temperature rise of the fiber in the vicinity of the input end for both the SMF and ZBLAN fibers. In particular, $\sim$10% of the power coupled into the ZBLAN fiber is estimated to be dissipated in the first meter length of the fiber, which is confirmed by the numerical simulation of the SC generation [20].

To further confirm the validity of our power handling model, we raise the core temperature to the fiber fuse temperature during the SC generation in the silica fiber. The experiments are carried out in the highly nonlinear (HiNL) silica fibers with an effective mode area of $\sim$10 μm^2 [5]. We couple light of up to $\sim$17 W average power ($\sim$6.3 kW peak power and pulsewidth $\sim$2 ns) with a continuous spectrum from $\sim$1.5 to 2 μm into a 40 cm length of HiNL fibers. By varying the input pump power and adjusting the corresponding pulse duty cycle, we vary the time-averaged power of the generated SC in the HiNL fiber from $\sim$2.4 to 15.2 W. We show that the SC average power increases linearly proportionally to the input pump power below the optical damage point, as illustrated in Fig. 9. When the SC average power is increased to 15.2 W SC average power, we observe a catastrophic backward propagating fiber fuse event starting from the HiNL fiber section after a short period of time. By using the aforementioned formula with a unit power dissipation of 10 W/m (i.e., 1 W power dissipated in the first 10 cm length of fiber as estimated by the simulation [5]) due to the high fiber nonlinearity, our model estimates the core temperature close to the input end of the HiNL fiber to be $\sim$1300–1400 K, which is close to the melting temperature of the silica glass of 1448 K and predicts a fiber fuse event. Hence, the theoretical result is consistent with the experimental observation and our thermal model is able to project the limit of the average power

Authorized licensed use limited to: IEEE Xplore. Downloaded on April 24, 2009 at 15:54 from IEEE Xplore. Restrictions apply.

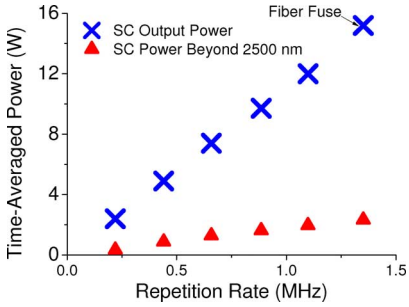

Fig. 9. Average SC output power scaling by varying pulse repetition rate and pump power in the HiNL fiber. (a) Total SC output power. (b) SC power beyond 2500 nm. A catastrophic fiber fuse event is observed when SC average power is measured to be 15.2 W.

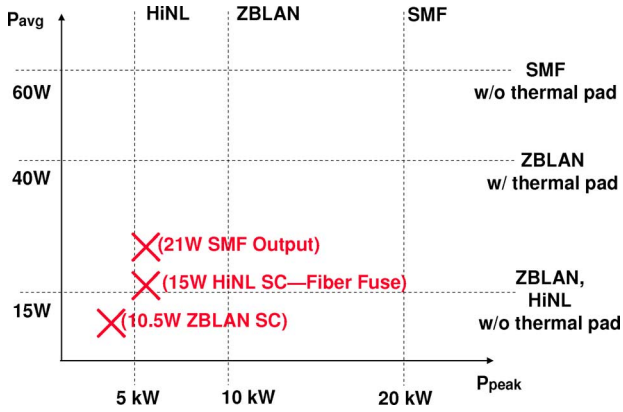

Fig. 10. Power handling limits for various fibers. Crossed data points represent the observed experimental data. The respective horizontal and vertical dashed lines of the specified fiber mark the operational boundary of the average and peak optical power.

handling of the fiber in SC generation. It should be noted that in the case of SC generation extending close to the intrinsic material absorption edge, the total thermal load in the fiber will be further increased, which will restrain the maximum power handling of the fiber.

For the SC generation in the standard ZBLAN fibers without extra thermal management, the maximum average power limit is simulated to be ~15 W with the assumption of 10% power dissipation in the first meter of the fiber as discussed earlier and an air convection coefficient of ~10 W/(m^2·K). In order to further scale up the SC power, better thermal management and heat dissipation techniques need to be implemented to reduce the core temperature of the fiber. One means is to wrap the optical fiber with a thermal pad with high thermal conductivity. As reported by [29], 42.8 W of pump power at 975 nm has been coupled into an erbium-doped ZBLAN fiber, which is held by an actively water-cooled fiber chuck as the heat dissipation means. We propose that by implementing the ZBLAN fiber with a 0.5-mm-thick thermal pad of a modest thermal conductivity, e.g., 1 W/(m·K), the maximum power handling can be increased to ~40 W. Therefore, increasing the average power of the SC generation in ZBLAN fibers beyond 10 W is feasible and achievable with sufficient thermal management.

To summarize the limitations of the power handling of different optical fibers, we plot the boundaries of the optical damage threshold as a function of both the peak power and average power in Fig. 10. As can be seen, both the SMF and ZBLAN SC cases reside within the boundaries of their respective peak and average power operating limits, and we have not observed any optical damage of the fibers during our experiments. On the other hand, the HiNL SC operates at a point that exceeds its calculated peak power and average power limits, and therefore, optical damage is expected.

VI. Spectral Bandwidth Limit of the SC Generation in ZBLAN Fiber

We calculate the long-wavelength edges of the SC spectrum in different ZBLAN fibers and match the theoretical results with experiments. Our calculations focus on the determining factors and system parameters that limit the long-wavelength edge of SC generation. Therefore, it can provide both an insight to the SC generation process and be used as a design tool for optimizing the SC generation.

Fundamentally, the SC generation is a nonlinear gain/loss process [1]. For the optical gain, there are a number of nonlinear optical interactions, including SPM, stimulated Raman scattering (SRS), and parametric FWM, present in the SC generation process [30]. Particularly, SPM of the MI-breakup short pulses is responsible for the initial spectral broadening in the SMF and ZBLAN fibers [5]. On the other hand, the Raman-scattering-assisted soliton self-phase shifting is one of the dominant mechanisms to redshift the SC spectrum and determine the long-wavelength edge in the ZBLAN fiber [5], [19], [20]. Despite the fact that SPM and SRS are different nonlinear processes, both of them are strongly affected by the effective mode area of the fiber A_{eff} and fiber length [30]. Since nonlinear effects become weaker when the effective mode area increases, the long-wavelength edge of the SC is impacted by the change of A_{eff}. We do not take the pump power into account because we generate our SC in different ZBLAN fibers under similar pump power.

The fiber loss, on the other hand, consists of the intrinsic absorption loss of the fiber material and the bend-induced loss determined by the fiber geometry, both of which are functions of wavelength. To take the fiber loss into consideration of the nonlinear generation process, we replace the fiber length by the effective interaction length, defined as $L_{\text{eff}} = [1 - \exp(-\alpha L)]/\alpha$, where α is the fiber loss [30]. For a step-index profile ZBLAN fiber, the effective mode area A_{eff} increases and effective fiber length L_{eff} decreases significantly when the wavelength shifts toward the long-wavelength, which reduces the nonlinear effects and will eventually stop the further wavelength shifting in the SC generation. Therefore, we hypothesize that the value of $L_{\text{eff}}/A_{\text{eff}}$ can be used to project the SC long-wavelength edge.

The effect mode area A_{eff} is calculated using the common definition of near-field mode effective area, which is [30]

$$A_{\text{eff}} = \frac{\left(\iint |\Psi(x,y)|^2\, dx\, dy\right)^2}{\iint |\Psi(x,y)|^4\, dx\, dy}.$$

Authorized licensed use limited to: IEEE Xplore. Downloaded on April 24, 2009 at 15:54 from IEEE Xplore. Restrictions apply.

TABLE I
FIBER PARAMETERS FOR BEND-INDUCED LOSS CALCULATION

Parameters	Description
α	amplitude loss factor
a	fiber core radius
$\Delta = \frac{n_{core} - n_{clad}}{n_{clad}}$	relative difference of refractive indices of the fiber core and cladding
R	radius curvature of the bended fiber
$V = k_0 a\sqrt{n_{core}^2 - n_{clad}^2}$	normalized frequency
u	$u = a\sqrt{n_{core}^2 k_0^2 - \beta^2}$
w	$w = a\sqrt{\beta^2 - n_{clad}^2 k_0^2}$
l	transverse mode index
$K_{l-1}(w), K_{l+1}(w)$	second kind of Bessel functions of the order $l-1$, and $l+1$
s	degeneracy factor

For the fundamental mode LP_{01}, of which the mode distribution is independent of azimuthal angle θ, the formula can be simplified in the cylindrical coordinates, which becomes

$$A_{\text{eff}} = 2\pi \frac{\left(\iint |\Psi(r)|^2 \, r \, dr\right)^2}{\iint |\Psi(r)|^4 \, r \, dr}$$

where Ψ is the transverse mode function, and the integration is conducted over all space.

We incorporate both the intrinsic material loss and fiber bend-induced loss into the calculation of the effective length L_{eff}. Material absorption loss is provided by the manufacturer of the ZBLAN fiber [31], which increases significantly toward the long-wavelength side. Bend-induced loss is the loss arising from the leakage of the laser transverse mode into the surrounding environment due to the curvature of the fiber. It has been studied analytically using the Maxwell's equations [32], [33] and can be calculated using the fiber parameters as

$$2\alpha = \frac{\sqrt{\pi}}{2s} \frac{(u/V)^2}{(a^2/2)K_{l-1}(w)K_{l+1}(w)} \frac{a \exp\left[(-4\Delta w^3/3aV^2)R\right]}{w\sqrt{(wR/a) + (V^2/2\Delta w)}}.$$

The descriptions of the fiber parameters are listed in Table I.

The radius curvature of the bended fiber is set to 40 cm in the simulation to match the experimental condition. Since we only consider fundamental mode LP_{11} in the fiber, both $K_{l-1}(w)$ and $K_{l+1}(w)$ degenerate to $K_1(w)$. The degeneracy factor is set to be 2 for the LP_{11} mode. The theoretical results of the bend-induced loss and material loss are then used to calculate the effective length.

We calculate the values of the effective mode area and effective fiber length in five ZBLAN fibers with different fiber design. The fiber characteristics of the ZBLAN fibers and the experimental SC long-wavelength edge defined as the 30 dB intensity drop from the flat part of the continuum are listed in Table II. All five fibers are made of the same materials, and thus possess the same material loss properties and fiber nonlinearities n_2. The wavelength dependence of the effective mode area and bend-induced loss of each fiber varies dramatically due to the difference in the fiber designs, as analyzed in the following paragraphs.

TABLE II
ZBLAN FIBER CHARACTERISTICS

Fiber #	Core Diameter	Cladding Diameter	Numerical Aperture	Length	SC Long Wavelength Edge
FL#1	8.9μm	125μm	0.21	7m	3.9μm
FL#2	10.6μm	125μm	0.20	15m	4.1μm
FL#3	5.7μm	125μm	0.16	15m	3.0μm
FL#4	8.6μm	125μm	0.17	8m	3.5μm
FL#5	7.0μm	125μm	0.30	8m	4.3μm

The calculated effective mode area A_{eff}, bend-induced loss, and effective length L_{eff} are illustrated in Fig. 11. As can be seen, the wavelength evolution of the calculated parameters has shown great disparities between different ZBLAN fibers due to their fiber designs. The mode field diameter and bend-induced loss increase most significantly in FL#3, which has the smallest core size and NA in all fibers. More specifically, the mode field area increases from ~37 μm^2 at 1.5 μm to over 1000 μm^2 at 4.5 μm, which leads to the dramatic increase of the bend-induced loss and plummeting of the effective length in the long-wavelength regime (see Fig. 11). Hence, the SC generation in the mid-IR regime is turned off. On the other hand, FL#5 has the tightest optical mode confinement that is manifested in the minimal change of the effective areas as the wavelength shifts toward the mid-IR. As a result, FL#5 demonstrates negligible bend-induced loss and has an effective length that is closer to its actual fiber length over a wide wavelength range. It should be noted that the bend-induced loss formula assumes infinite cladding size and does not take microbending of the optical fiber into account. Therefore, the actual fiber bend-induced loss is affected by the fiber fabrication process and may be higher than the theoretical value. FL#1 and FL#2, which are tested in the previous sections, have modest mode confinement, which is capable of guiding the mid-IR wavelength and supporting nonlinear wavelength generation to ~4 μm.

The theoretical values of $L_{\text{eff}}/A_{\text{eff}}$ are plotted in comparison with the experimental SC spectrum long-wavelength edges in Fig. 12. The SC long-wavelength edge is defined as the 30 dB amplitude drop from the flat part of the continuum. Therefore, the experimental SC long-wavelength edge is ~3.9, ~4.1, ~3.0, ~3.5, and ~4.3 μm for FL#1–FL#5, respectively, as illustrated in Fig. 12(a). It should be noted that the SC average power generated in different ZBLAN fibers in Fig. 12(a) varies from ~20 mW to over ~10.5 W due to the different pump laser systems. We have achieved >60% coupling efficiency from SMF to FL#1 and FL#2 and ~50% coupling efficiency for FL#5 due to the large mode mismatch. The calculated $L_{\text{eff}}/A_{\text{eff}}$ demonstrates the same wavelength evolution trend as the experiments. In particular, FL#3 has an $L_{\text{eff}}/A_{\text{eff}}$ value drop below 0.03 m/μm^2 around ~2.9–3 μm, while $L_{\text{eff}}/A_{\text{eff}}$ of FL#5 reaches the same value in the 4.3–4.4 μm region. Therefore, we fit the theoretical data with the experimental results and find out that the SC generation cuts off when the value of $L_{\text{eff}}/A_{\text{eff}}$ reduces to ~0.03 m/μm^2. The Raman amplification factor can be approximated by $G_A = g_R P L_{\text{eff}}/A_{\text{eff}}$, where g_R is the Raman

Authorized licensed use limited to: IEEE Xplore. Downloaded on April 24, 2009 at 15:54 from IEEE Xplore. Restrictions apply.

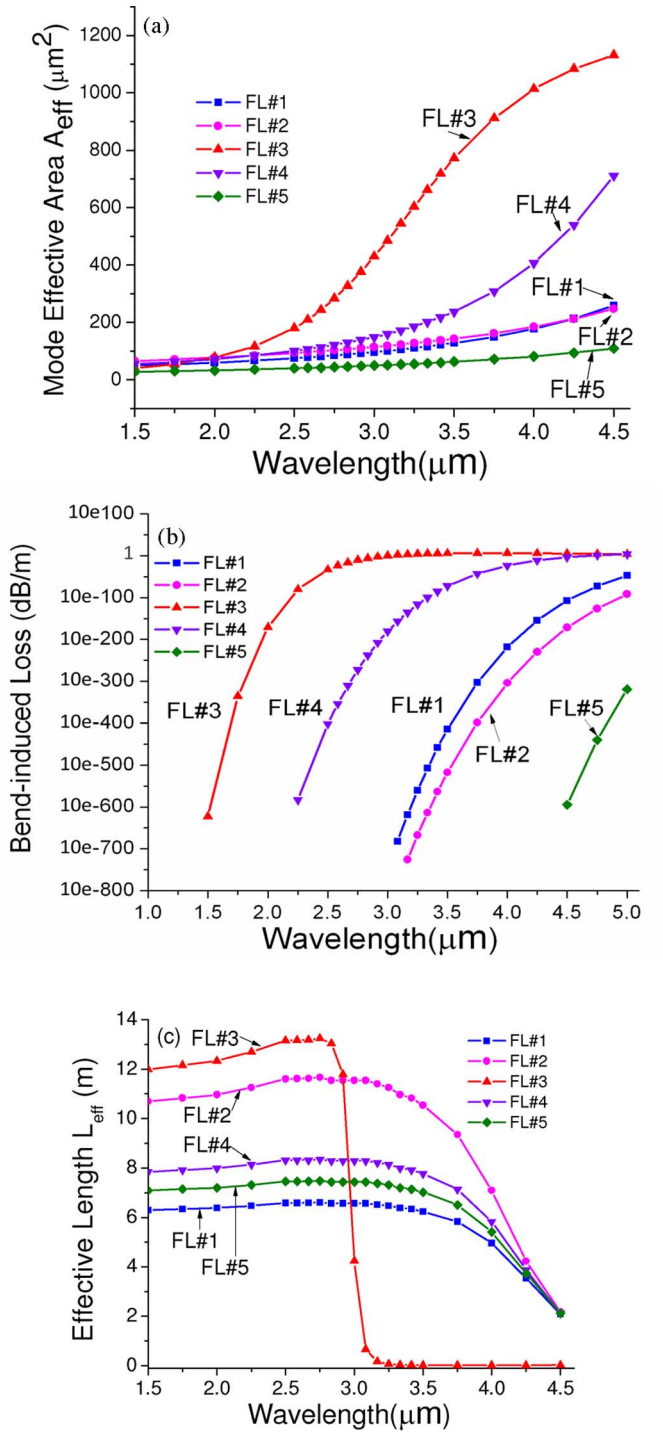

Fig. 11. Theoretical calculation. (a) Effective mode area A_{eff}. (b) Bend-induced loss. (c) Effective length L_{eff} in five ZBLAN fibers (FL#1–FL#5) with different fiber designs.

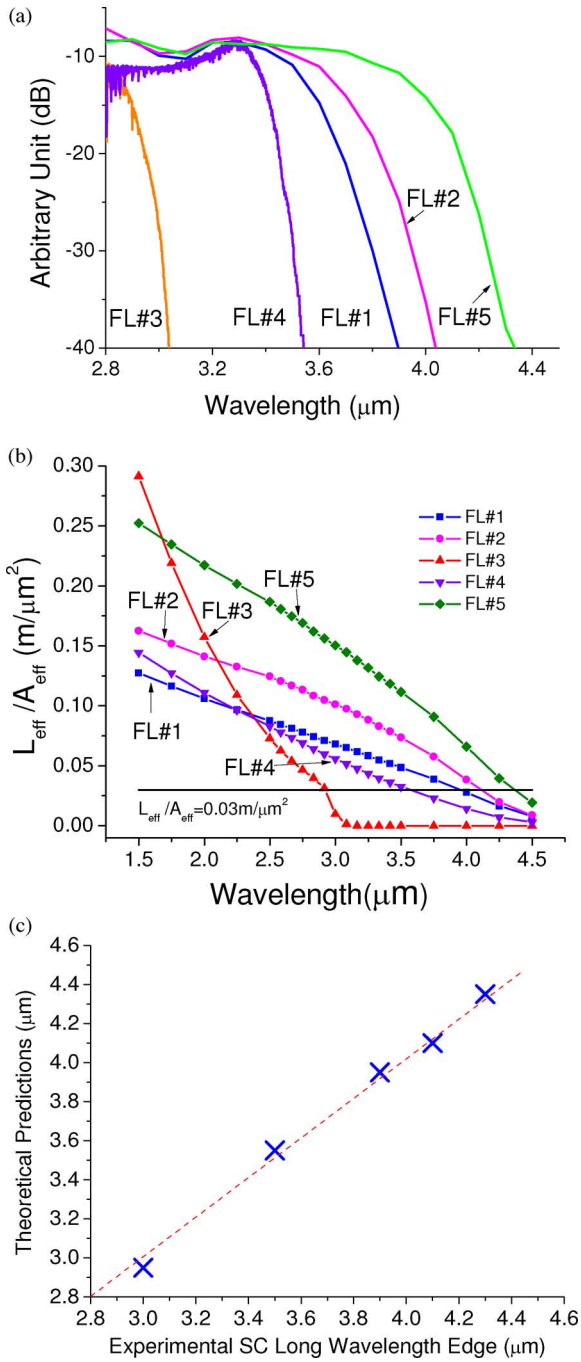

Fig. 12. Experimental and theoretical results in FL#1–FL#5. (a) Generated SC spectrum in the long-wavelength side. (b) Theoretical calculation of $L_{\text{eff}}/A_{\text{eff}}$. (c) Theoretical prediction of SC long-wavelength edge versus experimental data (dashed line represents the 45° angle fitting line).

gain coefficient and P is the pump peak power. We calculate G_A to be $\sim$10 assuming $P = 5$ kW, $g_R = 6.4 \times 10^{-14}$ m/W [20], and $L_{\text{eff}}/A_{\text{eff}} = 0.03$ m/μm^2, which is close to the Raman threshold [30]. Therefore, the value of $L_{\text{eff}}/A_{\text{eff}}$ can be used as a figure of merit to predict the SC long-wavelength edge. Fig. 12(c) illustrates the theoretical SC edge set by the $L_{\text{eff}}/A_{\text{eff}}$ fitting value versus the experimental results. We note that, for each pair of theoretical prediction and experimental observation, the SC long-wavelength edge disparity is within 50 nm, which confirms the validity of our hypothesis and theoretical model.

The most significant factor that limits the long-wavelength side growth of the SC spectrum varies between different fiber designs. We observe that the bend-induced loss in conjunction with the diminished nonlinear gain associated with the enlargement of the effective area limits the SC spectrum in FL#3 and

Authorized licensed use limited to: IEEE Xplore. Downloaded on April 24, 2009 at 15:54 from IEEE Xplore. Restrictions apply.

FL#4. For the fibers we used in the previous section, FL#1 and FL#2, nonlinear optical gain and fiber material loss play important roles to determine the SC long-wavelength edge. In particular, FL#1 has a shorter SC cutoff wavelength than that of FL#2 primarily due to the short fiber length even though these two fibers have similar mode effective area and bend-induced loss. On the other hand, for the SC generation in FL#5, the intrinsic material absorption of the fluoride glass clamps the SC generation to $\sim$4.5 μm.

Our calculation can be used to predict an optimal ZBLAN fiber design to extend the SC long-wavelength edge as far as possible. As demonstrated in our calculation, one of the most effective approaches is to employ a ZBLAN fiber with a large NA as well as a reasonably small core size, which can lead to a tighter confinement of the optical mode in the core region. Hence, not only the nonlinear wavelength generation process can be enhanced due to a smaller effective mode area, but the bend-induced loss will also be mitigated due to the reduced leakage of the more tightly confined optical mode. Therefore, we propose to generate the SC in a ZBLAN fiber with an NA of 0.30 and core diameter of 7 μm to extend the SC long-wavelength edge to $\sim$4.5 μm.

VII. Discussion and Conclusion

The all-fiber-integrated configuration improves the mechanical stability and the power efficiency of our SC light source. In the previous high-power SC experiments [20], we have used an erbium/ytterbium codoped cladding-pumped fiber laser with bulk optical coupling between different stages of the amplifier. The power efficiency from the pump diodes to the output in the SMF is $\sim$14%. In comparison, by splicing the amplifier stage together and removing the bulk optics, the pump-to-output efficiency is more than double of $\sim$30%. Under normal operation, the pump diode wall-plug electrical-to-optical efficiency is about 50% and the pump-to-SC conversion efficiency is $\sim$50% as discussed earlier. Therefore, the wall-plug electricity-to-SC power efficiency, defined as the ratio of the generated SC average power out of the total electrical power consumption, is improved to $>$7% for our SC light source from $<$3% for the tabletop system. To further improve the overall power efficiency of the system, the coupling efficiency of the mechanical splice needs to be increased, e.g., adding an intermediate fiber to better match the mode profile of the SMF and ZBLAN fibers. Moreover, the pump diodes of the last stage power amplifiers can be turned off during the long SC-OFF period in the modulated scenario to save the wall-plug electricity consumption.

Our SC light source is scalable in the time-averaged power up to 10.5 W by changing the pulse repetition rate. We show in Fig. 4 that the SC average power can be continuously varied by a factor of 7.5, i.e., from 1.4 to 10.5 W, by increasing the pulse repetition rate by the same scale from 0.42 to 3.33 MHz and increasing the pump power supply correspondingly. The power scalability is enabled by using the amplified laser diode pulses as the pump source for the SC generation. Compared to the conventional mode-locked lasers, our SC laser has a greater flexibility in the system configuration from the mature telecommunication technology and has potential scalability in the output power by adding more pump laser diodes.

In our experiments, the output time-averaged power is currently limited by the available pump power diodes coupled to the fiber amplifier. As a rule of thumb, one 8-W pump diode contributes $\sim$1 W average power to the SC generation. Therefore, we use twelve 8-W pump diodes in our pump system to generate the SC with $\sim$10.5 W output power. To further scale up the SC average power, more pump diodes need to be used to feed the fiber amplifier to generate a higher pump power. On the other hand, the SC long-wavelength edge is limited by the fiber nonlinearities, bend-induced loss, and fluoride material absorption. By using a ZBLAN fiber with step-index geometric design and fiber length, the SC spectral bandwidth can be pushed to the limit set by the ZBLAN material loss at $\sim$4.5 μm. Novel fiber geometry, e.g., photonic crystal fiber structure, could be used to better confine the optical mode area in the mid-IR in the future. To further extend the SC long-wavelength edge, new IR optical fiber, such as tellurite fiber, needs to be used. For example, SC generation extending to $\sim$5 μm is demonstrated in a tellurite fiber with photonic crystal structure [16].

In summary, mid-IR SC with 10.5 W time-averaged power and a continuous spectrum of $\sim$0.8–4 μm is generated in ZBLAN fibers by amplified nanosecond diode pulses. The average output power of the SC is linearly scalable from 1.4 to 10.5 W while maintaining the similar spectra by varying input pump power and the corresponding pulse duty cycle. We demonstrate modulation of the SC output pulse at 50% duty cycle with 1.5 and 7.7 kHz modulation speed by directly modulating the seed laser diode and controlling the amplifier gain. For the 10.5 W SC system, the long-wavelength edge at 4 μm is limited by the fiber length in combination with material absorption loss and bend-induced loss. By using a ZBLAN fiber with 0.3 NA and a core size of 7 μm, the SC long-wavelength edge can be further extended to $\sim$4.5 μm due to the minimized bend-induced loss and better confined effective mode area. We also simulate that time-averaged power of $\sim$15 W can be withheld in the standard ZBLAN fiber, and up to $\sim$40 W can be supported in the ZBLAN fiber with appropriate thermal management.

Acknowledgment

The authors thank Prof. A. Galvanauskas at the University of Michigan and Dr. G. Jacobovitz at Vyalex, Inc., for fruitful discussion.

References

[1] R. R. Alfano, *The Supercontinuum Laser Source: Fundamentals With Updated References*, 2nd ed. New York: Springer-Verlag, 2006.

[2] T. Morioka, K. Mori, S. Kawanishi, and M. Saruwatari, "Multi-WDM-channel, GBit/s pulse generation from a single laser source utilizing LD-pumped supercontinuum in optical fibers," *IEEE Photon. Technol. Lett.*, vol. 6, no. 3, pp. 365–368, Mar. 1994.

[3] H. Takara, "Multiple optical carrier generation from a supercontinuum source," *Opt. Photon. News*, vol. 13, no. 3, pp. 48–51, 2002.

[4] F. G. Omenetto, N. A. Wolchover, M. R. Wehner, M. Ross, A. Efimov, A. J. Taylor, V. V. R. K. Kumar, A. K. George, J. C. Knight, N. Y. Joly, and P. St. J. Russell, "Spectrally smooth supercontinuum from 350 nm to 3 μm in sub-centimeter lengths of soft-glass photonic crystal fibers," *Opt. Exp.*, vol. 14, pp. 4928–4934, 2006.

Authorized licensed use limited to: IEEE Xplore. Downloaded on April 24, 2009 at 15:54 from IEEE Xplore. Restrictions apply.

[5] C. Xia, M. Kumar, M. Y. Cheng, O. P. Kulkarni, M. N. Islam, A. Galvanauskas, F. L. Terry, M. J. Freeman, D. A. Nolan, and W. A. Wood, "Supercontinuum generation in silica fibers by amplified nanosecond laser diode pulses," *IEEE J. Sel. Topics Quantum Electron.*, vol. 13, no. 3, pp. 789–797, May/Jun. 2007.
[6] T. Izawa, N. Shibata, and A. Takeda, "Optical attenuation in pure and doped fused silica in their wavelength region," *Appl. Phys. Lett.*, vol. 31, pp. 33–35, 1977.
[7] J. C. Travers, A. B. Rulkov, B. A. Cumberland, S. V. Popov, and J. R. Taylor, "Visible supercontinuum generation in photonic crystal fibers with a 400W continuous wave fiber laser," *Opt. Exp.*, vol. 16, pp. 14435–14447, 2008.
[8] I. T. Sorokina and K. L. Vodopyanov, *Solid-State Mid-Infrared Laser Sources*. Berlin, Germany: Springer-Verlag, 2003.
[9] M. Razeghi, S. Slivken, Y. Bai, and S. R. Darvish, "The quantum cascade laser: A versatile and powerful tool," *Opt. Photon. News*, vol. 19, no. 7, pp. 42–47, 2008.
[10] K. Wille, "Synchrotron radiation sources," *Rep. Prog. Phys.*, vol. 54, pp. 1005–1067, 1991.
[11] G. S. Edwards, R. H. Austin, F. E. Carroll, M. L. Copeland, M. E. Couprie, W. E. Gabella, R. F. Haglund, B. A. Hooper, M. S. Hutson, E. D. Jansen, K. M. Joos, D. P. Kiehart, I. Lindau, J. Miao, H. S. Pratisto, J. H. Shen, Y. Tokutake, A. F. G. Van Der Meer, and A. Xie, "Free-electron-laser-based biophysical and biomedical instrumentation," *Rev. Sci. Instrum.*, vol. 74, pp. 3207–3245, 2003.
[12] R. R. Anderson, W. Farinelli, H. Laubach, D. Manstein, A. N. Yaroslavsky, J. Gubeli, K. Jordan, G. R. Neil, M. Shinn, W. Chandler, G. P. Williams, S. V. Benson, D. R. Douglas, and H. F. Dylla, "Selective photothermolysis of lipid-rich tissues: A free electron laser study," *Lasers Surg. Med.*, vol. 38, pp. 913–919, 2006.
[13] J. Mandon, E. Sorokin, I. T. Sorokina, G. Guelachvili, and N. Picqué, "Supercontinua for high-resolution absorption multiplex infrared spectroscopy," *Opt. Lett.*, vol. 33, pp. 285–287, 2008.
[14] S. A. Diddams, D. J. Jones, J. Ye, S. T. Cundiff, J. L. Hall, J. K. Ranka, R. S. Windeler, R. Holzwarth, T. Udem, and T. W. Hänsch, "Direct link between microwave and optical frequencies with a 300 THz femtosecond laser comb," *Phys. Rev. Lett.*, vol. 84, pp. 5102–5104, 2000.
[15] C. L. Hagen, J. W. Walewski, and S. T. Sanders, "Generation of a continuum extending to the midinfrared by pumping ZBLAN fiber with an ultrafast 1550-nm source," *IEEE Photon. Technol. Lett.*, vol. 18, no. 1, pp. 91–93, Jan. 2006.
[16] P. Domachuk, N. A. Wolchover, M. Cronin-Golomb, A. Wang, A. K. George, C. M. B. Cordeiro, J. C. Knight, and F. G. Omenetto, "Over 4000 nm bandwidth of mid-IR supercontinuum generation in sub-centimeter segments of highly nonlinear tellurite PCFs," *Opt. Exp.*, vol. 16, pp. 7161–7168, 2008.
[17] O. P. Kulkarni, C. Xia, D. J. Lee, M. Kumar, A. Kuditcher, M. N. Islam, F. L. Terry, M. J. Freeman, B. G. Aitken, S. C. Currie, J. E. McCarthy, M. L. Powley, and D. A. Nolan, "Third order cascaded Raman wavelength shifting in chalcogenide fibers and determination of Raman gain coefficient," *Opt. Exp.*, vol. 14, pp. 7924–7930, 2006.
[18] J. S. Sanghera, L. B. Shaw, C. M. Florea, P. Pureza, V. Q. Nguyen, D. Gibson, F. Kung, and I. D. Aggarwal, "Non-linearity in chalcogenide glasses and fibers, and their applications," presented at the Quantum Electron. Laser Sci. Conf. (QELS 2008), San Jose, CA, May 4–9, Paper QTuL5.
[19] C. Xia, M. Kumar, O. P. Kulkarni, M. N. Islam, F. L. Terry Jr., M. J. Freeman, M. Poulain, and G. Mazé, "Mid-infrared supercontinuum generation to 4.5 μm in ZBLAN fluoride fibers by nanosecond diode pumping," *Opt. Lett.*, vol. 31, pp. 2553–2555, 2006.
[20] C. Xia, M. Kumar, M.-Y. Cheng, R. S. Hegde, M. N. Islam, A. Galvanauskas, H. G. Winful, F. L. Terry Jr., M. J. Freeman, M. Poulain, and G. Mazé, "Power scalable mid-infrared supercontinuum generation in ZBLAN fluoride fibers with up to 1.3 watts time-averaged power," *Opt. Exp.*, vol. 15, pp. 865–871, 2007.
[21] G. Canat, J. Mollier, J. Bouzinac, G. M. Williams, B. Cole, L. Goldberg, Y. Jaouën, and G. Kulcsar, "Dynamics of high-power erbium–ytterbium fiber amplifiers," *J. Opt. Soc. Amer. B*, vol. 22, pp. 2308–2318, 2005.
[22] B. C. Stuart, M. D. Feit, S. Herman, A. M. Rubenchik, B. W. Shore, and M. D. Perry, "Optical ablation by high-power short-pulse lasers," *J. Opt. Soc. Amer. B*, vol. 13, pp. 459–468, 1996.
[23] B. C. Stuart, M. D. Feit, S. Herman, A. M. Rubenchik, B. W. Shore, and M. D. Perry, "Nanosecond-to-femtosecond laser-induced breakdown in dielectrics," *Phys. Rev. B*, vol. 53, pp. 1749–1761, 1996.
[24] S. I. Yakovlenko, "Physical processes upon the optical discharge propagation in optical fiber," *Laser Phys.*, vol. 16, pp. 1273–1290, 2006.
[25] E. M. Dianov, I. A. Bufetov, A. A. Frolov, V. M. Mashinsky, V. G. Plotnichenko, M. F. Churbanov, and G. E. Snopatin, "Catastrophic destruction of fluoride and chalcogenide optical fibres," *Electron. Lett.*, vol. 38, pp. 783–784, 2002.
[26] E. Sonntag, C. Borgnakke, and G. J. Van Wylen, *Fundamentals of Thermodynamics*. New York: Wiley, 1998.
[27] J. M. Parker, "Fluoride glasses," *Annu. Rev. Mater. Sci.*, vol. 19, pp. 21–41, 1989.
[28] J. A. Harrington, "Infrared fibers," in *Handbook of Optics,* vol. 3*, Classical, Vision & X-ray Optics*, M. Bass, J. M. Enoch, E. W. Van Striland, and W. L. Wolfe, Eds. Washington, DC: Optical Society of America, 2002, pp. 14.1–14.16.
[29] X. Zhu and R. Jain, "10-W-level diode-pumped compact 2.78 μm ZBLAN fiber laser," *Opt. Lett.*, vol. 32, pp. 26–28, 2007.
[30] G. P. Agrawal, *Nonlinear Fiber Optics*, 3rd ed. San Diego, CA: Academic, 2001.
[31] Fluoride fiber SMFF [Online]. Available: http://www.fiberlabs.co.jp/fiber_smff(E).htm
[32] J.-I. Sakai and T. Kimura, "Bending loss of propagation modes in arbitrary index profile optical fibers," *Appl. Opt.*, vol. 17, pp. 1499–1506, 1978.
[33] D. Marcuse, "Curvature loss formula for optical fibers," *J. Opt. Soc. Amer.*, vol. 66, pp. 216–220, 1976.

Chenan Xia received the B.S. degree in physics in 2004 from Fudan University, Shanghai, China, and the M.S. degree in electrical engineering in 2006 from the University of Michigan, Ann Arbor, where he is currently working toward the Ph.D. degree in electrical engineering.

His current research interests include fiber-based mid-infrared supercontinuum light source and its applications on spectral fingerprinting, biomedical diagnosis, and fiber-to-the-home passive optical network.

Zhao Xu received the B.S. degree in electronic engineering from Tsinghua University, Beijing, China, in 2006. He is currently working toward the Ph.D. degree in electrical engineering at the University of Michigan, Ann Arbor.

His current research interests include supercontinuum generation in mid-infrared and its applications.

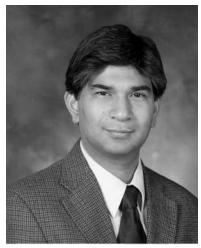

Mohammed N. Islam (M'94–SM'96–F'05) received the B.S., M.S., and Sc.D. degrees from Massachusetts Institute of Technology, Cambridge, in 1981, 1983, and 1985, respectively, all in electrical engineering.

From 1985 to 1992, he was a member of the Technical Staff in the Advanced Photonics Department, AT&T Bell Laboratories, Holmdel, NJ. In 1992, he joined the Department of Electrical Engineering and Computer Science, University of Michigan, Ann Arbor, where he is currently a Full Tenured Professor. He has authored or coauthored over 115 papers published in refereed journals, and holds over 124 patents or patents pending. In addition, he has authored three books and has written several book chapters. His current research interests include mid-infrared laser sources and their applications in fiber-to-the-home, advanced semiconductor process control, combustion monitoring, infrared counter-measures, chemical sensing, biomedical selective laser ablation, and ultrahigh-resolution imaging of automobile parts, such as power train components. He is also engaged in research on modulators and new architectures for fiber to the home systems. He teaches a number of courses including introduction to photonics, fiber optic communications, high-tech entrepreneurship, and patent fundamentals for engineers. He has also founded several spin-off companies from the University of Michigan, including Xtera Communications, Celeste Optics, AccuPhotonics, and Cheetah Omni. He also founded Omni Sciences, Inc., Ann Arbor, MI, where he is currently the Founder and Chief Technology Officer (CTO). He is also a CTO-Optics at Coherix, Inc., Ann Arbor, MI.

Authorized licensed use limited to: IEEE Xplore. Downloaded on April 24, 2009 at 15:54 from IEEE Xplore. Restrictions apply.

Prof. Islam was a Fannie and John Hertz Fellow from 1981 to 1985. In 1992, he was awarded the Optical Society of America (OSA) Adolf Lomb Medal for pioneering contributions to nonlinear optical phenomena and all-optical switching in optical fibers. He also received the U-M Research Excellence Award in 1997. He became a Fellow of the OSA in 1998. In 2002, he received the Texas eComm Ten Award for being one of the ten most influential people in Texas's digital economy. He is also the first recipient of the prestigious 2007 Distinguished University Innovator Award for developing and commercializing break-through technology as well as bringing lessons learned back into the classroom through teaching of entrepreneurship and intellectual property protection. He has also been an Invited Speaker at over 60 conferences and symposia, and a member of numerous Conference Technical Committees, Advisory Committees, and Board of Directors. He is also a Registered Patent Agent with the US Patent and Trademark Office.

Fred L. Terry, Jr. (S'78–M'80–SM'99) received the B.S., M.S., Ph.D. degrees from Massachusetts Institute of Technology, Cambridge, in 1981 and 1985, respectively, all in electrical engineering.

He was engaged in research on the electronic properties of ammonia-annealed silicon dioxide films (nitrided oxides). He joined the Department of Electrical Engineering and Computer Science, University of Michigan, Ann Arbor, where he is currently a Professor. He was engaged in research on low-temperature deposition of high-quality insulators for MIS devices on Si, InP, and GaAs, InP HFET device fabrication and physics, deep submicrometer etch processes, and processes for high-temperature Si MOS operation and operation in ionizing radiation environments. His current research interests include include nondestructive and *in situ* thin-film characterization techniques including spectroscopic ellipsometry and reflectometry, control of semiconductor processes and equipment, sensing systems for process control, and plasma etch and deposition processes.

Prof. Terry is a member of the Electron Devices Society of the IEEE, the American Physical Society, and the Sigma Xi.

Mike J. Freeman, photograph and biography not available at the time of publication.

Andy Zakel, photograph and biography not available at the time of publication.

Jeremiah Mauricio, photograph and biography not available at the time of publication.

Authorized licensed use limited to: IEEE Xplore. Downloaded on April 24, 2009 at 15:54 from IEEE Xplore. Restrictions apply.